Simultaneously High Stiffness and Damping in Nanoengineered Microtruss Composites

Julien Meaud, Trisha Sain, Bongjun Yeom, Sei Jin Park, Anna Brieland Shoultz, Gregory Hulbert,* Zheng-Dong Ma, Nicholas A. Kotov,* A. John Hart,* Ellen M. Arruda,* and Anthony M. Waas‡,*

College of Engineering, University of Michigan, Ann Arbor, Michigan 48109, United States. ‡Senior author. All students and postdocs contributed equally to the contents of this paper.

ABSTRACT Materials combining high stiffness and mechanical energy dissipation are needed in automotive, aviation, construction, and other technologies where structural elements are exposed to dynamic loads. In this paper we demonstrate that a judicious combination of carbon nanotube engineered trusses held in a dissipative polymer can lead to a composite material that *simultaneously* exhibits both high stiffness and damping. Indeed, the combination of stiffness and damping that is reported is quite high in any single monolithic material. Carbon nanotube (CNT) microstructures grown in a novel 3D truss topology form the backbone of these nanocomposites. The CNT trusses are coated by ceramics and by a nanostructured polymer film assembled using the layer-by-layer technique. The crevices of the trusses are then filled with soft polyurethane. Each constituent of the composite is accurately modeled, and these models are used to guide the manufacturing process, in particular the choice of the backbone topology and the optimization of the mechanical properties of the constituent materials. The resulting composite exhibits much higher stiffness (80 times) and similar damping (specific damping capacity of 0.8) compared to the polymer. Our work is a step forward in implementing the concept of materials by design across multiple length scales.

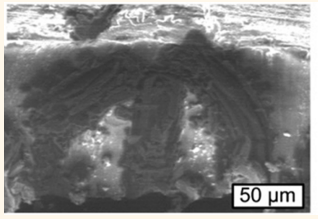

KEYWORDS: integrated manufacturing · stiffness · damping · carbon nanotube · polymer nanocomposites · hierarchical structures

Most engineering structures are designed to have high stiffness and strength. However in response to dynamic loads the damping capacity is equally important, and classical materials exhibit a trade-off between stiffness and damping. For example, steel and diamond are very stiff but exhibit poor capacity to dissipate energy; on the other hand, materials with high damping such as rubber and other elastomeric materials have a very low stiffness. An age-old materials challenge has been to produce an engineered material that exhibits high stiffness and damping simultaneously. In this paper we show that materials design starting with appropriately selected nanoscale building blocks can result in a composite material with significantly higher stiffness than conventional "lossy" polymers while maintaining high damping.

The presence of structural hierarchy within natural and man-made materials and its effect on bulk material properties has been an important focus of the materials research community since the early 1990s.[1−3] The hierarchical particulate composites with coated spheres morphology and the "rank two morphology" proposed by Lakes[4] is one such hierarchy that can lead to improved stiffness and damping. However, preserving the mechanical properties as one moves up in length scale (*e.g.*, from nanometer to micrometer) is a critical challenge for practically relevant macroscale materials.[5−9] Understanding the effects of hierarchical structure can guide the *ab initio* synthesis of new materials and thereby can result in desired mechanical properties.[1,10,11] We selected a stiff nanoscale engineered carbon nanotube truss and a lossy surrounding material with a judiciously designed truss structure to attain *high stiffness* and *high damping simultaneously*.[12−17] The manufacturability of the laminate-based architecture and the compatibility between the carbon nanotube (CNT) microtruss and the surrounding viscoelastic layer give the resulting composite attractive macroscale properties and pave the way for future practical aplications.

The problem of preserving the mechanical properties as one builds up the

* Address correspondence to hulbert@umich.edu, kotov@umich.edu, ajhart@mit.edu, arruda@umich.edu, dcw@umich.edu.

Received for review December 15, 2013 and accepted March 12, 2014.

Published online March 12, 2014
10.1021/nn500284m

hierarchy has been resolved in the present work by using a designed topology of carbon nanotube based truss structures and subsequent optimization of it. The exceptional ability to control the manufacturing of these building blocks (CNT microtruss and layer-by-layer (LBL) composite layer) allows a simulation-based *material-by-design* approach and reduces the processing and fabrication times compared to conventional nanocomposite manufacturing. Carbon nanotubes have been investigated as reinforcements for polymer nanocomposites because of their extreme stiffness.[18−20,22] However early work did not take full advantage of the properties of the CNTs due to lack of organization at scales much larger than the nanoscale of the CNTs. Nanocomposites made of CNT forests filled with an elastomer have been shown to exhibit an anisotropic response with properties similar to a foam material when compressed in the direction of the fillers.[21] Recent studies have shown that scalable and reproducible three-dimensional microstructures can be fabricated using vertically aligned CNTs.[23,32] Utilization of these microstructures, referred to as CNT pillars, to form a nanocomposite with organization at the nano- and microscale and with macroscale dimensions remains unachieved. We produced nanocomposites using a hierarchical combination of carbon nanotube based truss design and layer-by-layer nanomanufacturing. Manufacturing and fabrication of complicated 3D geometry are always a critical challenge one needs to consider for large-scale manufacturing of nanocomposites. Therefore, in the present work, an integrated computational modeling approach that simulates the material response at each and every step of the manufacturing process in a finite element framework is presented. Thus one can avoid the expensive and time-consuming manufacturing trials by performing numerical experiments effectively within this computational framework.

Previous studies have shown a LBL-assembled clay-nanocomposite film[23] that exhibits remarkable stiffness enhancement at the macroscale (thickness of a few micrometers). However, even though LBL deposition has advantages in fine control of intermolecular interaction between matrix and fillers, fabrication of macroscale thick film using the LBL method requires a significant amount of time in most cases. We demonstrate here that excellent compressive stiffness can be obtained at larger length scales (with out-of-plane dimensions approaching 1 mm) and in a time-efficient manner using a hierarchical design with a CNT backbone microstructure coated with an LBL nanocomposite film. Using the concept of spatial strain amplification, which results from the material inhomogeneity, the proposed nanocomposites acquire orders of magnitude improvement in stiffness compared to the pristine polymer without any loss in damping.

RESULTS AND DISCUSSION

The nanocomposites contain a specially designed backbone topology of carbon nanotube microstructure based columns (CNT pillars) that are reinforced with an alumina shell. The pillars are then coated with an LBL clay-polyurethane layer (PU/clay). The crevices in this topology are filled with a lossy PU synthesized as described in the Supporting Information (SI). This core structure is sandwiched between steel sheets, and this repeat unit is stacked to a desired thickness to produce a layered nanocomposite. The core elements and particles have dimensions in the nanometer range, while the CNT columns have height in the micrometer range. The in-plane dimensions of the overall composite are 5−10 mm; the out-of-plane dimension is 0.65 to 0.85 mm. Combining two different length scales in manufacturing gives rise to a hierarchical structure within the material with a very attractive combination of stiffness and damping.

To facilitate the design, each constituent in the hierarchy is modeled in a finite element framework and experimentally validated. Computational models are developed to predict the stiffness and damping of these composites. Extensive parametric studies are performed to show the best possible pathway toward achieving high stiffness and high damping. Designing one such material system is a fundamental building block toward scalable advanced manufacturing. This approach may well provide a unified framework for integrated design and manufacturing of synthetic materials. The optimum design of the microarchitecture has been found through numerical analysis. In response to a sinusoidal load, the stress and strain are out of phase for a viscoelastic material. The tangent of the phase angle, commonly called tan δ (also known as loss tangent or loss factor), is a measure of the damping capacity of the material.[13] For the initial nanocomposite design, 2D finite element models were built to predict the dynamic stiffness and tan δ, in response to a sinusoidal load (see SI for details). In order to evaluate the best candidate microarchitectures for composites with high stiffness and high damping, we investigated several topologies that could be manufactured using CNT pillars. Results from simulations for the composites are shown in a stiffness-loss map (in which the effective dynamic modulus is plotted as a function of the effective loss factor) in Figure 1c. A composite with straight pillars behaves like the Voigt topology analyzed by Chen and Lakes,[12] exhibiting very high stiffness but low damping. Altering the straight pillars with curved geometry and arranging them in certain configurations can increase the damping with a moderate loss of stiffness. Parametric studies showed that by varying the stiffness of CNT pillars from 1 GPa to 1TPa, as shown in Figure 1e, a value of 100 GPa stiffness produces the best combination of stiffness and

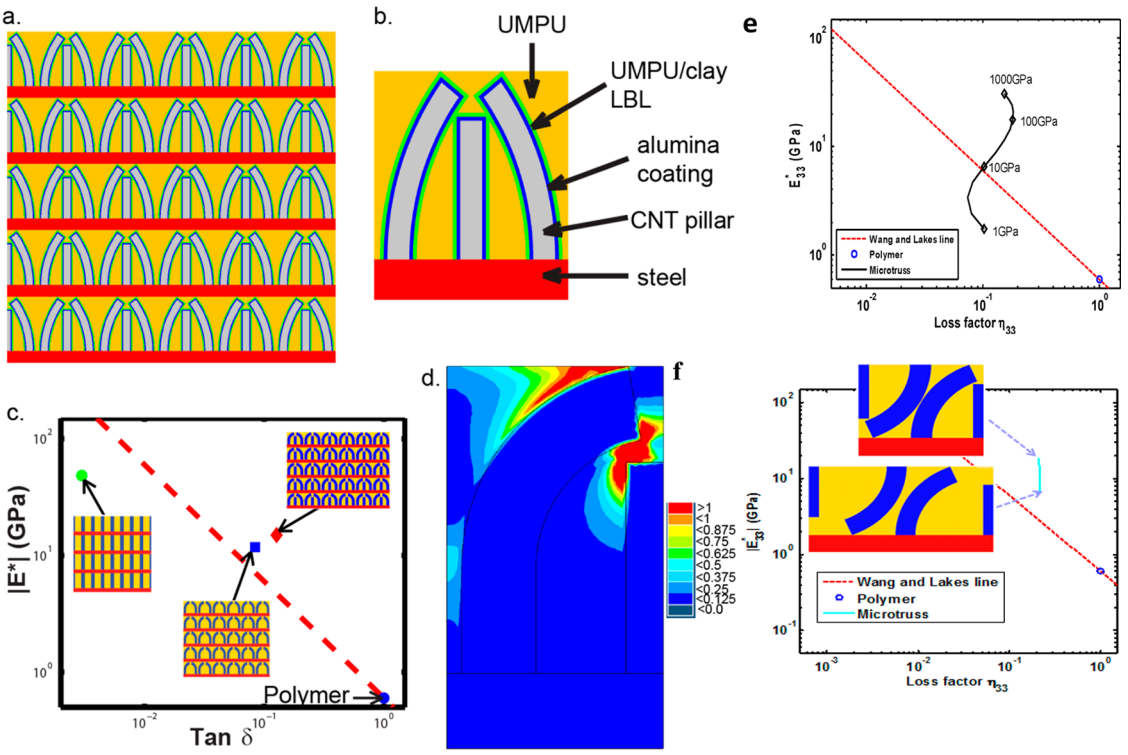

Figure 1. (a) Schematic representation of the composite in 2D. The composites are intended to be loaded in compression in the vertical direction. (b) Unit cell of the composite: red corresponds to metal sheets, gray to CNT pillars, blue to alumina coating, green to PU/clay LBL, and yellow to PU. (c) Stiffness-loss map of 2D topologies. Blue circle corresponds to the properties of the filling polymer, chosen to lie on the Wang and Lakes line $|E^*| \tan \delta = 0.6$ GPa. (d) Contour plot of the mechanical energy dissipation, showing the high dissipation between the straight pillars and the curved pillars due to the high shear strains in the polymer matrix. (e) Effect of CNT pillar stiffness on nanocomposite property plotted on stiffness-loss map, FE parametric study. (f) Effect of gaps between CNT pillars on nanocomposite property plotted on stiffness-loss map, FE parametric study.

damping for the nanocomposite. Similarly another set of parametric studies, as shown in Figure 1f, informed us that by optimizing the gap filled with polymer, higher stiffness can be achieved without any reduction in damping. The final configuration of having a straight pillar within two curved pillars was considered from finite element (FE) simulations, resulting in combined high stiffness and high damping, keeping in mind the viability of manufacturing.

Viscoelastic polymers dissipate energy by shear deformation, and this may be enhanced by altering the microarchitecture of the composites, to achieve localized high-energy dissipation regions. In comparison to straight pillars, curved pillars arranged in a microtruss topology induce strain concentration in the polymer, resulting in higher damping with a moderate reduction in stiffness. Further improvement, both in the stiffness and damping, was observed by adding a straight pillar between the curved pillars. Adding a straight pillar in the middle improves the volume fraction of the CNT pillars and improves stress transfer. Additionally, shear deformation of the polymer increases significantly due to the constraint effect by the pillar arrangement near the corners, enhancing damping. The contour plot of the dissipated energy per cycle, shown in Figure 1d, demonstrates that significant energy dissipation is introduced in the space between the straight pillars and the curved pillars in this most complex topology.

Figure 2a shows the comparison between the experimental data and FE model prediction for uniaxial loading/unloading at a quasi-static rate (0.005/s). The FE prediction shows excellent capability of the constitutive models to capture the entire hysteresis loop for pure PU and PU/clay. A significant improvement in stiffness compared to pure PU (30−50 times) is observed as the clay volume fraction increases in PU/clay composites (Figure 2b). Earlier work has shown that adding clay particles to the polymer using the LBL process significantly improved stiffness properties.[23,26,27,31] However, the improvement in stiffness due to addition of stiffer clay particles is usually associated with a reduction in damping, which is seen in Figure 2c. It has also been shown[26,27,29] that the nanocomposite becomes brittle, and damping decreases significantly with a clay volume fraction of around 12%. This suggests maintaining the clay volume fraction at around 10−12% while manufacturing the PU/clay samples. In order to estimate the

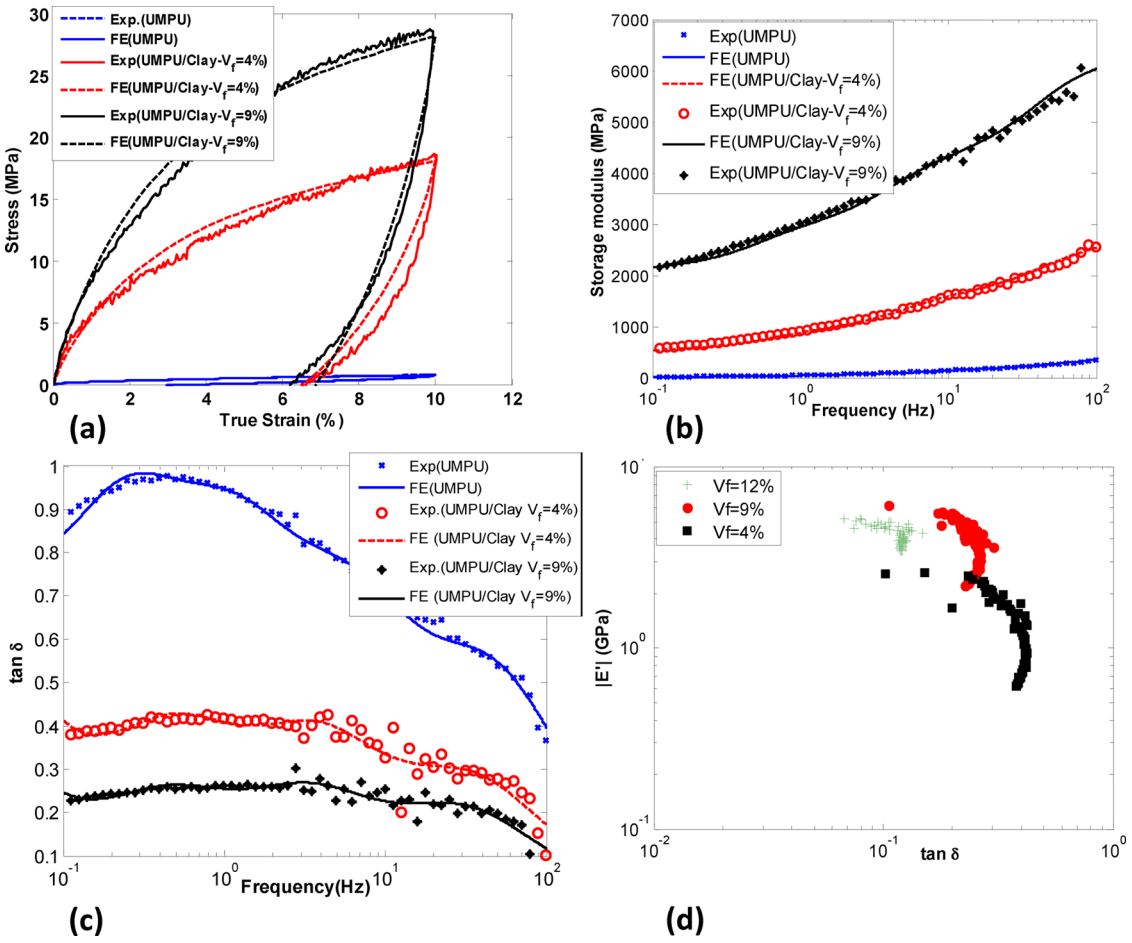

Figure 2. (a) Uniaxial loading−unloading response of PU and PU/clay composites for different clay V_f % at quasi-static rate (0.005/s). (b) Comparison between FE model prediction and experimental frequency-dependent storage modulus variation for PU and PU/clay composites. (c) Comparison between FE model prediction and experimental frequency-dependent tan δ variation for PU and PU/clay composites. (d) DMA results for different V_f % of clay in the stiffness-loss map.

optimum performance of the PU/clay nanocomposites in terms of combined stiffness and damping properties, the experimental storage modulus and tan δ values are plotted in a stiffness-loss map for different volume fractions in Figure 2d. It is observed that V_f = 9% has the best combination of stiffness and damping properties, and hence this was chosen to be the candidate material for coating the CNT truss.

Toward manufacturing the final composite, first a single-layer alumina-coated microtruss sample filled with PU is tested under nanoindentation (as shown in Figure 3c). The geometry of the samples considered was as follows: a single layer of dimensions 10×10 mm^2 with 40 μm diameter microtrusses, leading to the final composite manufactured by sandwiching three such layers, resulting in a thickness of 850 μm for the layered composite with in-plane cross section dimensions of 10×10 mm^2 (as shown in Figure 3b). The single-layer sample was tested using a spherical indentor of diameter 150 μm under load control. The final composite was subsequently tested to assess properties in a tension−compression mechanical machine manufactured by Kammath and Weiss (Supporting Information). A macromeasurement was chosen instead of nanoindentation in order to determine homogenized (on the scale of several repeat geometrical unit cells) properties rather than local pointwise properties. Dynamic mechanical analysis (DMA) measurements were not considered because of their low resolution. The sandwiched composite was loaded and unloaded in cyclic compression at a constant displacement rate of 0.5 μm/s (corresponding to a strain rate of 6×10^{-4}/s). The load-deformation curves were recorded from both the tests, and stress−strain values were calculated once the cyclic response was stabilized after three cycles of loading/unloading of both the samples, resulting in the plots shown in Figure 3e and f.

For the triangular loading pulse used in these experiments, damping cannot be measured in terms of the tangent of the phase angle. However, an energy-based definition of damping, the specific

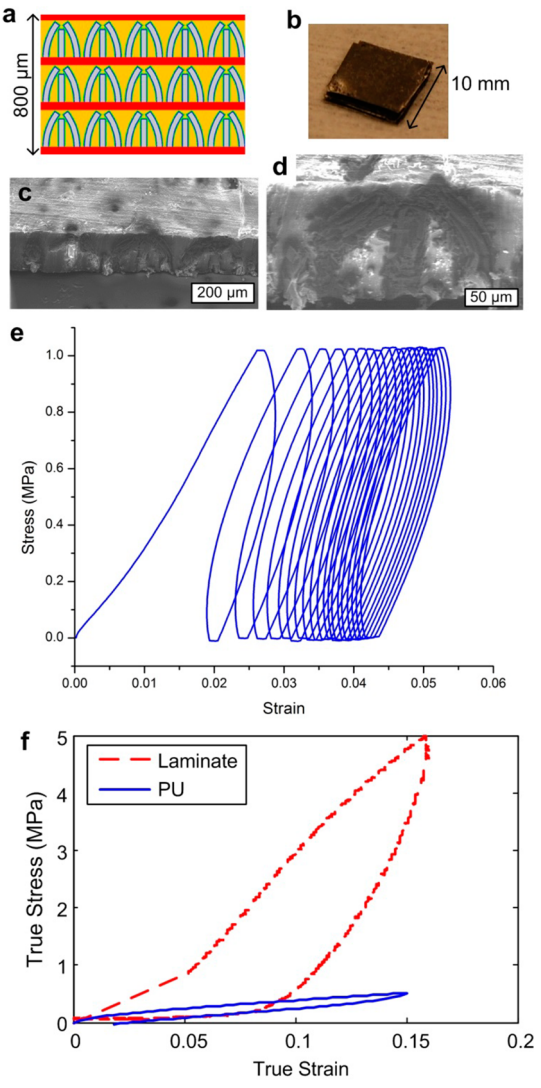

Figure 3. (a) Schematic representation of the composite in 2D. (b) Image of the final sandwiched composite. (c) SEM image of a single-layer 40 μm CNT truss filled with PU. (d) SEM image showing the cross section of the single-layer nanocompsoite filled with polymer and coated with PU/clay LBL. (e) Stress–strain response of single-layer nanotruss under nanoindentation. (f) Stress–strain response for the final composite compared with PU stress–strain response.

damping capacity (denoted as ψ), can be used.[28] Specific damping capacity ψ is defined as the ratio of the dissipated energy per cycle to the stored energy. The dissipated energy per cycle is given by the area within the loading/unloading curve. The stored energy is given by the enclosed area of the triangle connecting the origin, the point on the curve corresponding to maximum strain, and the projection of this point on the horizontal axis. To compute the stiffness of the truss sample from the loading/unloading curve, the slope of the unloading curve is used.

It is observed that the composite has considerably higher stiffness than the pristine PU for both the single-layer and the final sandwiched composite. The stiffness of the PU with the same loading condition was found to be 2.3 MPa. It increased to 318 MPa for the single-layer and 204 MPa for the sandwiched specimen. Moreover, the damping of PU (ψ = 0.54) was maintained in the case of the final sandwiched structure (ψ = 0.54) even though it was slightly lower in the single-layer specimen (ψ = 0.45). The difference between the single-layer measurement and the final sandwich composite is due to the different test setups used, as an indentation test used for the single-layer specimen measures only relatively local material response depending on the indenter location; hence it is usually different from the global macroscopic response. It is highly possible that the indenter tip directly touches the microtruss and therefore provides a much stiffer response and lower damping. Further, the final sandwich composites may have manufacturing variability between successive layers, resulting in variation in response.

Imperfections in the manufacturing process, such as the presence of PU between the top of the CNT pillars and the metal sheets, could cause a drop in the stiffness and an increase in the damping. For these reasons theoretical simulations are expected to be an upper bound for the stiffness and a lower bound for the damping. The important point to note here is that even with manufacturing imperfections the composite has significant improvement in stiffness properties (80-fold for the 40 μm CNT truss) without losing any damping of the base PU. As explained earlier the chosen microtruss topology enhances shear dissipation within the PU, and hence damping does not decrease as much as one expects in a traditional Voigt topology. For this particular set of samples the damping of the pristine PU was preserved in the final sandwiched composite. However our model prediction shows that by increasing the CNT stiffness and reducing the gap between successive CNT pillars one can actually improve both the stiffness and damping of the final composites (as shown in Figure 3), and the resulting composite response (with CNT pillar stiffness being 1 TPa, composite stiffness can be 30 GPa and damping about 0.6) can exceed the traditional bounds estimated by Lakes.

CONCLUSIONS

The present methodology shows a way of successfully scaling up nanomanufacturing processes, starting from the nanoscale to the macrolevel. The study shows an enhancement in stiffness of up to 80 times can be achieved without a detriment to the damping of the polymer. Numerical parametric studies demonstrate that further improvements in stiffness without loss of damping could be achieved by optimizing the stiffness of the CNT pillars (by ALD coating) and the gap between the CNT pillars. This particular approach of combining the chemical process optimization and

nanomanufacturing guided by computational modeling is indeed a step forward toward implementing the concept of materials by design across multiple length scales.

METHODS/EXPERIMENTAL DETAILS

A method for direct growth of 3D CNT microstructures was developed to produce the desired complex truss topology. As-grown curved CNT pillars were produced, using a TiN underlayer to hinder the growth of CNT pillars in selected portions (see Figure 4a). A parametric study was performed in which the TiN regular catalyst overlap area was varied to select the resulting geometry that was the closest to the designed architecture (see Figure 4b). Once the selection was made, a large array of the selected design was patterned and fabricated. The details of the growth process include the catalyst patterning consisting of two repetitions of photolithography and deposition steps, as the TiN underlayer needs to be patterned before regular CNT growth catalyst (10 nm of Al_2O_3 and 1 nm of Fe). First a desired geometry of TiN is patterned onto a Si wafer with 300 nm of a SiO_2 layer using photolithography with an SPR220 photoresist. Then the 500 Å TiN layer is deposited on the patterned wafer by reactive sputtering. Lift-off is performed by immersing the wafer in acetone and sonicating twice. Once the two sonication steps are completed, the wafer is rinsed in 2-propanol twice, then dried. The second photolithography step defines the geometry of the regular CNT growth catalyst. Then the catalyst is deposited by electron beam evaporation, and lift-off procedures are performed again to prepare the wafer for CNT growth. CNT growth is performed in a hot-wall furnace using a thermal chemical vapor deposition (thermal CVD) process. The wafer is diced to an appropriate size and is placed in a 22 mm inner diameter quartz tube with sealed endcaps for isolated growth gas flow. The sample is subjected to an annealing step (10 min ramp to 775 °C and 10 min hold at 775 °C) during 100 sccm of H_2 and 400 sccm of He flow. During the growth step, 100 sccm of C_2H_4 is added to the total flow. The duration of the growth step determines the height of the CNT microstructures. Two minutes of growth step produces ~100 μm tall CNT microstructures, which are what are used in this study. Once the growth step is completed, the furnace is cooled while the growth gases are still flowing to improve the adhesion of the CNT microstructures to the substrate. Figure 4c shows an array of as-grown curved CNT microtrusses, which have been used to build the final composite.

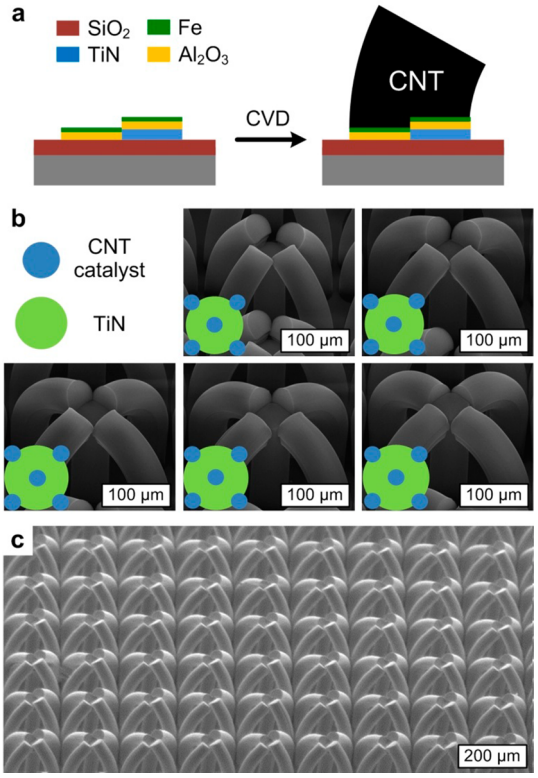

Figure 4. (a) Schematic representation of how the TiN underlayer can be used to create as-grown curved CNT pillars. (b) CNT microstructure topology optimization by varying the overlap of TiN and CNT catalyst. (c) Large array of CNT microtrusses. (d) CNT microstructures embedded in a PU film after heat pressing showing a flat top and no excess PU layer on top.

Higher stiffness is usually accompanied by a loss of damping. However, increasing the CNT pillar stiffness initially results in a simultaneous increase in the stiffness and damping of the composite (see SI). The increase in damping is due to the high shear strains in the polymer. This necessitated the effort to maximize the stiffness of the CNT pillars by reinforcing with other materials. Due to the ability to create a conformal coating on the CNTs and to penetrate into the porous CNT pillars, atomic layer deposition (ALD) of Al_2O_3 was selected as the reinforcing scheme.[24,30] The penetration depth of the Al_2O_3 coating into the CNT pillars was studied, and the CNT pillar dimensions were optimized to maximize the stiffness. Once the CNT microstructures were grown to appropriate height and shape, the sample was subjected to 1000 cycles of ALD of Al_2O_3. A shell of alumina of thickness 5 to 10 μm is formed on the outside of the CNT pillars. Optimization of the alumina deposition led to a 30−50-fold increase in the effective stiffness of the CNT pillars (from 1 to 15 ± 7.5 GPa for 40 μm diameter CNT pillars and 50 ± 15 GPa for 20 μm diameter CNT pillars).

To maximize dissipation of mechanical energy, PU with high damping was synthesized as the base constituent for the LBL nanocomposite layer and filler material. Since the intrinsic mechanical property of polyurethane can be tuned by selective choice among various kinds of diisocyantes and diols, a lossy PU was prepared to have high damping property in the frequency range of 0.1 to 1 Hz at room temperature. While the loss factor of PU was considerably increased by adjusting the molecular ratio of soft and hard segments to be almost equal, the stiffness of PU decreased as a consequence of the high soft segment content, poly(tetramethylene ether) glycol. In order to enhance the stiffness of PU, the LBL assembly method was utilized to build PU/clay nanocomposite films. It was found that the effective properties of the overall composite were improved when the LBL coating on the CNT pillars was included in the simulation compared to a model with PU fill only (as shown in Figure 1 in the SI). Hence the 3D CNT trusses were coated with an LBL layer, and a significant improvement in the stiffness was observed.

The PU samples were prepared using 4,4′-methylene bis(phenyl isocyanate) (MDI) as hard segment and poly(tetramethylene ether) glycol (PTMG) as soft segment. 2,2-Dimethyl-1,3-propanediol (DMPD) was used as chain extender. MDI was dissolved in *N*-methyl-2-pyrrolidone (NMP), then heated to 60 °C. PTMG (M_n = 1000 g mol^{-1}) was injected and stirred under a nitrogen atmosphere with reflux. After 2 h of reaction, prepolymer was extended with DMPD for 1 h. Then, 3-diethylamino-1,2-propanediol (DEAPD) was added to complete the chain extension followed by quternization with dimethyl sulfate to impart positive charge. In order to obtain PU with high damping at room temperature, the weight ratio between hard segment and soft segment was finely tuned to be almost the same. Therefore, the molar ratio of MDI:PTMG:DMPD was fixed to be 3:1:2, which was 49% of the hard segment content in total weight. For DMA testing, a PU solution was casted onto a Teflon substrate, followed by heating to remove the solvent.

The PU has been mechanically characterized through a set of experiments to understand its frequency and strain amplitude dependent stiffness and damping variation. The PU has a very low stiffness (storage modulus ~48 MPa) and a high loss factor (tan δ = 0.95) measured *via* dynamic mechanical analysis at a frequency of 1 Hz at room temperature. A constitutive model was developed to capture the experimental DMA response over a wide frequency range.[25] The constitutive model is based on a finite strain nonlinear viscoelastic framework to capture the large elastic deformation of the polymer network. Numerical values of the model parameters are listed in Table 1 of the SI.

PU/clay LBL films were prepared on glass substrates using layer-by-layer self-assembly. The clay dispersion was prepared after 1 week of stirring 0.5% MTM clay dispersed in DI water. The substrate was immersed in the PU and MTM clay dispersion for 5 min and rinsed two times with DI water followed by drying. The deposition cycle was repeated 300 times to produce 300 bilayers of nanocomposite film on a glass slide. Then, it was immersed in 0.5% HF aqueous solution to peel off the LBL film from the substrate. Finally, the free-standing PU/clay LBL film was obtained.

PU is added by drop-casting an excessive amount of PU dispersed in NMP (20% PU by wt) to make sure that all the voids within the microtrusses are filled. The sample is then left on a hot plate set at 100 °C for 8 h in a fume hood to evaporate the solvent. Once the solvent has evaporated, the excess polymer layer protruding above the top of the CNT microtrusses was removed by heat pressing. Once the top of the PU film is level with the top of the CNT microtrusses, the PU film is delaminated from the Si substrate and the edges not containing CNT microtrusses are cut off. The steel facesheets are sheared to the same size, and the sandwich laminate is prepared by stacking the facesheets and the PU films and heat pressing again.

Due to the considerable time needed to make the LBL samples with the desired thickness, a complete fill with PU/clay was not considered. Instead the alumina-coated CNT pillars were further coated with 5 μm thick LBL layers, and the crevices in the microtruss were filled with PU. The process of embedding reinforced CNT pillars in PU and creating a freestanding CNT/PU composite film is explained in the last section of the SI. The entire three-dimensional hierarchical nanocomposites were modeled accurately, by considering constitutive descriptions of each of the constituents (see the SI).

Conflict of Interest: The authors declare no competing financial interest.

Acknowledgment. The authors gratefully acknowledge financial support from DARPA (Grant HR0011-10-C-0192) (Dr. A. Lazarus); Dr. Matt Maschmann and Jeff Baur (AFRL) for mechanical characterization; Sameh Tawfick (University of Michigan) for assistance with CNT fabrication and ALD; Michael De Volder (IMEC) for discussions about fabrication of the CNT microtruss geometrics; Dr. Shiv Joshi (NextGen Aeronautics, Inc.) for project oversight; and Bret Kitcher (University of Michigan) for all the PU and PU/clay experiments.

Supporting Information Available: Details on the numerical simulations are explained in the Supporting Information. This information is available free of charge *via* the Internet at http://pubs.acs.org.

Note Added after ASAP Publication: This paper published ASAP on March 18, 2014. Several additional corrections were made in the Abstract, Results and Discussion, and the Conclusion, and the revised version was reposted on March 25, 2014.

REFERENCES AND NOTES

1. Lakes, R. S. Materials with Structural Hierarchy. *Nature* **1993**, *361*, 511–515.
2. Tai, K.; Dao, M.; Suresh, S.; Palazoglu, A.; Ortiz, C. Nanoscale Heterogeneity Promotes Energy Dissipation in Bone. *Nat. Mater.* **2007**, *6*, 454–462.
3. White, A. A.; Best, S. M.; Kinloch, I. A. Hydroxyapatite–Carbon Nanotube Composites for Biomedical Applications: A Review. *Int. J. Appl. Ceram. Technol.* **2007**, *4*, 1–13.
4. Lakes, R. S. High Damping Materials: Effect of Structural Hierarchy. *J. Compos. Mater.* **2002**, *36*, 287–296.
5. Treacy, M. M.; Ebbsen, T. W.; Gibson, J. M. Exceptionally High Young's Modulus Observed for Individual Carbon Nanotubes. *Nature* **1996**, *381*, 678–681.
6. Breuer, O.; Sundararaj, U. Big Returns from Small Fibers: A Review of Polymer/Carbon Nanotube Composites. *Polym. Compos.* **2004**, *25*, 630–645.
7. Van Lier, G.; Alsenoy, C. V.; Van Doren, V.; Geerlings, P. *Ab Initio* Study of the Elastic Properties of Single-Walled Cabon Nanotubes and Graphene. *Chem. Phys. Lett.* **2000**, *326*, 181–185.
8. Manevitch, O. L.; Rutledge, G. C. Elastic Properties of a Single Lamella of Montmorillonite by Molecular Dynamics Simulations. *J. Phys. Chem.* **2004**, *108*, 1428–1435.
9. Sturcova, A.; Davies, G. R.; Eichorn, S. J. Elastic Modulus and Stress Transfer Properties of Tunicate Cellulose Whiskers. *Biomacromolecules* **2005**, *6*, 1055–1061.
10. Sigmund, O. A New Class of Extremal Composites. *J. Mech. Phys. Solids* **2000**, *48*, 397–428.
11. Sigmund, O. Tailoring Material with Prescribed Elastic Properties. *Mech. Mater.* **1995**, *20*, 351–368.
12. Chen, C. P.; Lakes, R. S. Analysis of High Loss Viscoelastic Composites. *J. Mater. Sci.* **1993**, *28*, 4299–4304.
13. Lakes, R. S. *Viscoelastic Materials*; Cambridge University Press, 2009.
14. Brodt, M.; Lakes, R. S. Composite Materials Which Exhibit High Stiffness and High Viscoelastic Damping. *J. Compos. Mater.* **1995**, *29*, 1823–1833.
15. Gibiansky, L. V.; Lakes, R. S. Bounds on the Complex Bulk and Shear Moduli of a Two-Dimensional Two Phase Viscoelastic Composites. *Mech. Mater.* **1997**, *25*, 79–95.
16. Meaud, J.; Sain, T.; Hulbert, G. M.; Waas, A. M. Analysis and Optimal Design of Layered Composites with High Stiffness and High Damping. *Int. J. Solids Struct.* **2013**, *50*, 1342–1353.
17. Lakes, R. S.; Lee, T.; Bersie, A.; Wang, Y. C. Extreme Damping in Composite Materials with Negative Stiffness Inclusions. *Nat. Mater.* **2001**, *410*, 565–567.
18. Yu, M. F.; Lourie, O.; Dyer, M. J.; Moloni, K.; Kelly, T. F.; Ruoff, R. S. Strength and Breaking Mechanism of Multiwalled Carbon Nanotubes Under Tensile Load. *Science* **2000**, *287*, 637–640.
19. Wang, X.; Bradford, P.; Liu, W.; Zhao, H.; Inoue, Y.; Yuan, F. G.; Zhu, Y. T. Mechanical and Electrical Property Improvement in CNT/Nylon Composites through Drawing and Strectchin. *Compos. Sci. Technol.* **2011**, *71*, 1677–1683.
20. Mittal, V. *Polymer Nanotube Nanocomposites: Synthesis, Properties, and Applications*; Wiley, 2010.
21. Carey, B. J.; Patra, P. K.; Myung, G. H.; Ajayan, P. M. Foam Like Behavior in Compliant Continuously Reinforced Nanocomposites. *Adv. Funct. Mater.* **2013**, *15*, 45–50.
22. Mack, J. J.; Viculis, L. M.; Ali, A.; Luoh, R.; Yang, G.; Hahn, H. T.; Ko, F. K.; Kaner, R. B. Graphite Nanoplatelet Reinforcement of Electrospun Polyacrylonitrile Nanofibers. *Adv. Mater.* **2005**, *17*, 77–80.
23. Podsiadlo, P.; Kaushik, A. K.; Kotov, N.; Arruda, E. M.; Waas, A. M. Ultrastrong and Stiff Layered Polymer Nanocomposites. *Science* **2007**, *318*, 80–83.
24. De Volder, M.; Tawfick, S. H.; Park, S. J.; Copic, D.; Zhouzhou, Z.; Lu, W.; Hart, A. J. Diverse 3D Microarchitectures Made by Capillary Forming of Carbon Nanotubes. *Adv. Mater.* **2010**, *22*, 4384–4389.
25. Sain, T.; Meaud, J.; Waas, A. M.; Arruda, E. M. Rate Dependent Finite Strain Constititutive Modeling of Polyurethane and Polyurethane Based Clay Nanocomposites. *Int. J. Solids Struct.*Manuscript in preparation.
26. Li, Y.; Waas, A. M.; Arruda, E. M. A Closed-Form, Hierarchical, Multi-interphase Model for Composites—Derivation, Verification and Application to Nanocomposites. *J. Mech. Phys. Solids* **2011**, *59*, 43–63.
27. Kaushik, A. K.; Waas, A. M.; Arruda, E. M. A Constitutive Model for Finite Deformation Response of Layered

Polyurethane-Montmorillonite Nanocomposites. *Mech. Mater.* **2011**, *43*, 186–193.
28. Martz, E. O.; Lakes, R. S.; Park, J. B. Hysteresis Behaviour and Specific Damping Capacity of Negative Poisson's Ratio Foams. *Cell. Polym.* **1996**, *15*, 349–364.
29. Ray, S. S.; Okamoto, M. Recent Progress in Synthesis and Evaluation of Polymer-Montmorillonite Nanocomposites. *Prog. Polym. Sci.* **2003**, *28*, 1539–1545.
30. Puurunen, R. L. Surface Chemistry of Atomic Layer Deposition: A Case Study for the Trimethylaluminum/Water Process. *J. Appl. Phys.* **2005**, *97*, 301–352.
31. Arruda, E. M; Boyce, M. C. A Three Dimensional Constitutive Model for the Large Stretch Behavior of Rubber Elastic Materials. *J. Mech. Phys. Solids* **1993**, *41*, 389–412.
32. Iijima, S. Helical Microtubules of Graphite Carbon. *Nature* **1991**, *354*, 56–58.